MRI: Quantitative Evaluation of Diseased Tissue by Viscoelastic Imaging Systems

39

Mikio Suga

Abstract

Magnetic resonance elastography (MRE) and ultrasound elastography (USE) are imaging techniques that non-invasively quantify the mechanical properties of tissue by using magnetic resonance imaging and ultrasound imaging systems. In this study, we aim to develop a system that can quantitatively obtain details such as the viscoelasticity of small organs and tissues in the body by using clinical magnetic resonance imaging (MRI) and MR microscopy. By evaluating MRE and USE using a soft tissue-equivalent gel phantom with a known viscoelastic coefficient, we aim to investigate the characteristics of both devices and promote their standardization. The purpose of this study is to confirm the frequency characteristics of the developed phantom and optimize the scatterer material for ultrasound measurement. We confirmed that the phantoms are in good agreement with a physical model of the liver, and the developed phantoms are considered effective for the quantitative assessment of the MRE and USE systems.

Keywords

Magnetic resonance imaging · Magnetic resonance elastography · Ultrasound elastography · Phantom Quantitative assessment

39.1 Introduction

The mechanical property of a tissue is related to physiological and pathological states. Magnetic resonance elastography (MRE) and ultrasound elastography (USE) are imaging techniques that non-invasively quantify the mechanical properties of tissue by using magnetic resonance imaging and ultrasound imaging systems [1, 2]. It is expected that measuring the mechanical properties of tissues will be useful in the diagnosis of diseases such as hepatic fibrosis and cancer. MRE visualizes shear-wave patterns within a tissue using a modified phase-contrast MR sequence. In order to generate shear waves within the tissue, external vibration systems are used (Fig. 39.1). The local quantitative values of tissue viscoelasticity (stiffness) are calculated from the shear-wave pattern by using an inversion algorithm [3–5]. We have been developing an MRE system using clinical MRI and MR microscope for measuring viscoelasticity at multi-scale and multi-frequency (Fig. 39.2) [6, 7].

The measured viscoelasticity can be used as an imaging biomarker [8]. A quantitative phantom is required to assess the accuracy and repeatability of elastography systems. We have been developing tough and stable polyacrylamide (PAAm) gel phantoms for this purpose [9–12]. We developed a phantom with viscoelasticity close to that of living tissue by using glycerin as a solvent. For ultrasonic measurements, a scatterer is necessary for the phantom. The material and concentration of the scatterer are related to the stability of ultrasonic measurement and uniformity of the MRI image.

In this study, we compared the mechanical properties of our phantoms with those of living tissue and optimized the scatterer material and concentration for ultrasound measurement with the developed MRE system and commercial USE system.

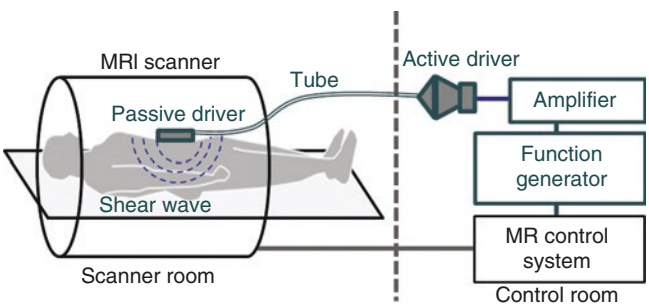

Fig. 39.1 Schematic of the MR elastography system

M. Suga (✉)
Center for Frontier Medical Engineering, Chiba University, Chiba, Japan
e-mail: mikio.suga@faculty.chiba-u.jp

M. Hashizume (ed.), *Multidisciplinary Computational Anatomy*, https://doi.org/10.1007/978-981-16-4325-5_39

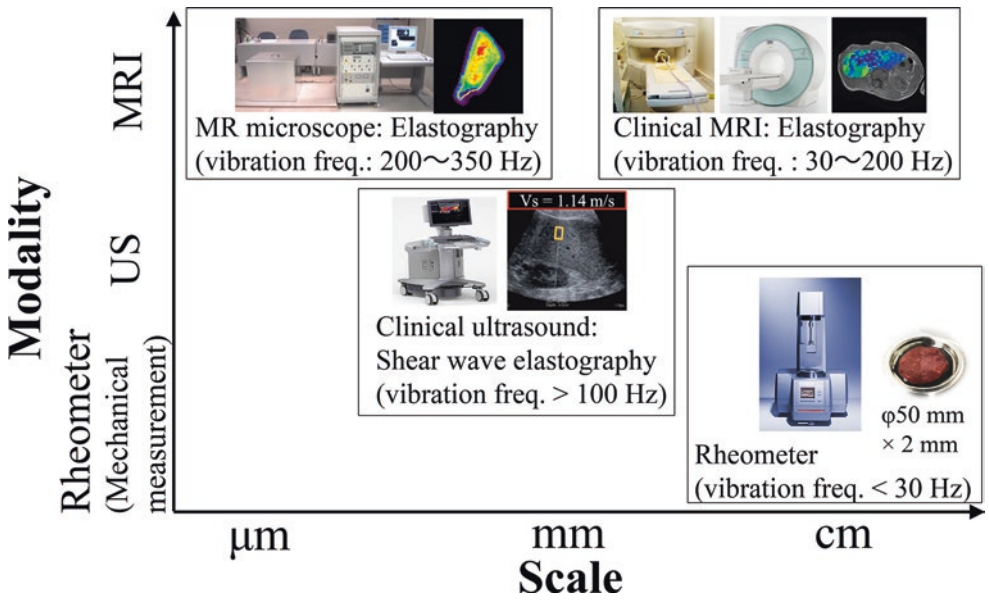

Fig. 39.2 Multi-modality equipment for measuring viscoelasticity at multi-scale and multi-frequency

Table 39.1 Rheometer measurement parameters

Frequency	Hz	1–30
Strain amplitude	%	1
Normal force	N	0.7
Diameter	mm	50
Thickness	mm	1.5–2.0 (phantom) 2.0–2.7 (liver)
Temperature	°C	23

39.1.1 Development of a Tissue-Mimicking Viscoelastic Phantom for Quantitative Assessment of MRE

We fabricated gel phantom sheets with high loss moduli (G''). The phantom sheets were designed to have a storage modulus (G') of 1.5 kPa and a loss tangent ($\tan\delta = G''/G'$) greater than 0.2 at 60 Hz [13]. The storage and loss moduli of the phantom and a fresh in vitro bovine liver were measured using a parallel-disc rheometer (MCR302, Anton-Parr). We repeated the measurements on these three samples with the strain amplitude set to 1% (Table 39.1).

The phantom (diameter: 120 mm, height: 150 mm) was measured with MRE using 3-T MRI (MAGNETOM Skyra, Siemens) at 30, 40, 50, and 60 Hz (Table 39.2) by spin-echo-EPI-MRE pulse sequence (work in progress) and the vibration from a pneumatic driver system with active driver to a passive driver to create the shear wave in the phantom. The passive driver with a diameter of 18 cm was placed on the center of the phantom. The fresh in vitro bovine liver (width: 135 mm, height: 70 mm, length: 250 mm) was measured with MRE using 0.3-T MRI (Hitachi) at 31.25, 62.5, 100, and 200 Hz (Table 39.3) by spin-echo-EPI-MRE pulse sequence (a motion encoding gradient (MEG) was added to SE-EPI using the sequence development environment of Hitachi) and ultrasound system (ACUSON S3000, Siemens) with virtual touch IQ (VTIQ). At high-frequency measurement of the fresh in vitro bovine liver (width: 15 mm, depth: 15 mm, height: 50 mm), MRE using 1-T MR microscope (MR-MICRO, MRTecnology) was used (Table 39.4).

To evaluate the temporal changes, the phantom designed to have a storage modulus of 3 kPa was examined by MRE for the duration of 1 year.

Table 39.2 Multi-frequency MRE imaging parameters by 3-T MRI

Sequence		Spin-echo-EPI-MRE (work in progress)			
Vibrational frequency	Hz	30	40	50	60
Repetition time (TR)	s	4.5	4.5	3.0	3.0
Echo time (TE)	ms	97			
FOV	mm^2	384 × 384			
Matrix size	pixel	128 × 128			
Pixel size	mm	3			
Number of slices		15			
Slice thickness	mm	3			
Temperature	°C	23			

Table 39.3 Multi-frequency MRE imaging parameters by 0.3-T MRI

Sequence		Spin-echo-EPI-MRE			
Vibrational frequency	Hz	31.25	62.5	100	200
Repetition time (TR)	s	4.8			
Echo time (TE)	ms	67			
FOV	mm^2	348 × 348			
Matrix size	pixel	116 × 116			
Pixel size	mm	3			
Number of slices		15			
Slice thickness	mm	3			
Temperature	°C	23			

Table 39.4 MRE imaging parameters by 1-T MR microscope

Sequence		Spin-echo-MRE
Vibrational frequency	Hz	200
Repetition time (TR)	s	0.5
Echo time (TE)	ms	21
FOV	mm^2	25 × 25
Matrix size	pixel	128 × 128
Pixel size	mm	0.2
Number of slices		1
Slice thickness	mm	1.8
Average		3
Temperature	°C	23

Table 39.5 SWE measurement parameters

Probe		9 MHz linear (9 L4)	
Depth range	cm	0.3–4.0	
Detect pulse	MHz	6.0	
Method		VTIQ	VTQ
ROI size	mm^2	1.5 × 1.5	5 × 5
Push pulse	MHz	4.4, 5.7	4.0
Number of measurement		4 × 3	5
Depth	cm	2	
Temperature	°C	22	

39.1.2 Ultrasound-Based Shear-Wave Speed Measurement on a Highly Viscous Embedded Phantom

The PAAm gel is composed of a three-dimensional network polymer and a large amount of liquid. The storage modulus (stiffness) of the PAAm gel depends mainly on the quantity of acrylamide. Additionally, the density of the three-dimensional network polymer depends mainly on the quantity of cross-linker. The loss modulus (viscosity) depends mainly on the ratio of water and glycerin. To make compatible phantoms for MRE and USE, the aluminum oxide powder was added to the PAAm gel for the scatterer.

A highly viscoelastic embedded phantom was measured with US-based shear-wave elastography (SWE). The phantom composed square soft part (background part; width: 130 mm, depth: 130 mm, height: 160 mm) and embed two cylindrical hard parts (embedded part; length: 130 mm, diameter: 10 mm and 20 mm). The weight percent of acrylamide in the embedded part is 1.5 times higher than the background part. In addition, we have created a homogeneous phantom that is content the same as the embedded part.

The SWS was measured with virtual touch quantification (VTQ) and VTIQ (Table 39.5). VTQ provides only single-point SWS measurement, and VTIQ provides two-dimensional color-coded SWE (2D SWE), which displays 2D color velocity maps and allows for multiple measurements to be obtained. The stiffness is proportional to squaring of the SWS.

We measured the embedded parts, and the background parts were 5 mm apart from the outline of the embedded ones. VTIQ measurements were repeated 4 points on the same depth and three times at each part, VTQ measurements were repeated five times at each part, and the mean value and SD of the SWS were calculated. Reference values of the embedded part were measured in a homogenous phantom made with the same material component. The reference value of the background part was measured at a deeper area of the embedded phantom.

39.2 Results

39.2.1 Development of a Tissue-Mimicking Viscoelastic Phantom for Quantitative Assessment of MRE

Figure 39.3 shows the stiffness (square root of the sum of squares of the storage and loss modulus) obtained with MRE, the rheometer, and USE. The stiffness of the phantom and bovine liver increased with frequency. Figure 39.4 shows the change in the mechanical properties of the phantom over a year. The change in the storage and loss modulus during the 1-year period was within ±3%.

39.2.2 Ultrasound-Based Shear-Wave Speed Measurement on a Highly Viscous Embedded Phantom

Table 39.6 shows the SWS in the embedded part and background part. In the background part, the SWS was equivalent to the reference value. The SWS of the embedded part with a diameter of 20 mm in a highly viscous phantom was measured accurately with the SWE; however, with a diameter of 10 mm was lower than the reference value. Figure 39.5 shows the B-mode image and the VTIQ image around the embedded part with a diameter of 10 mm. On the VTIQ image, the embedded part was demarcated from the background; however, the border was not sharp. In addition, the embedded part on the VTIQ was visualized to be larger than the part on the B-mode image. This phantom has the potential to be used as a quality control phantom to mimic living tissues.

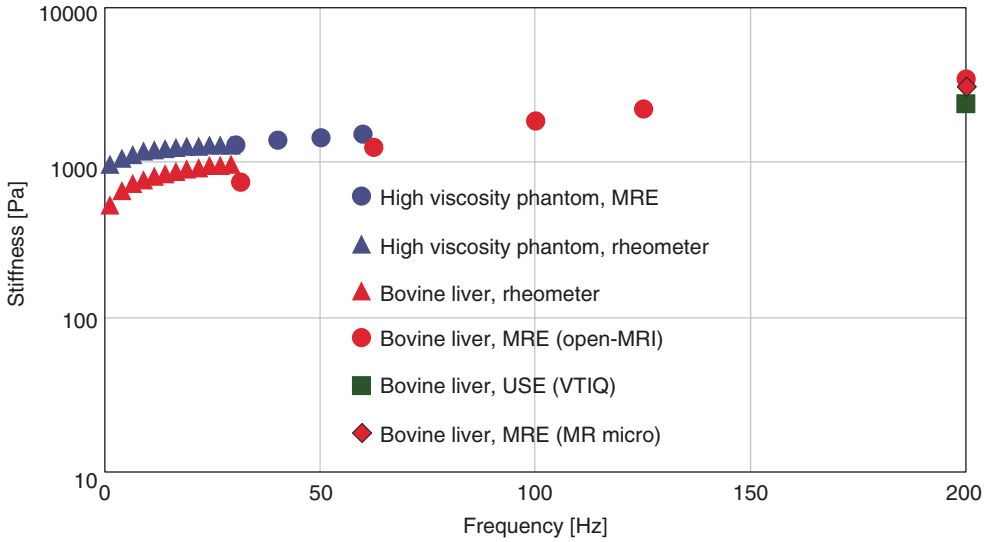

Fig. 39.3 Frequency characteristics of gel phantoms and in-vitro bovine liver

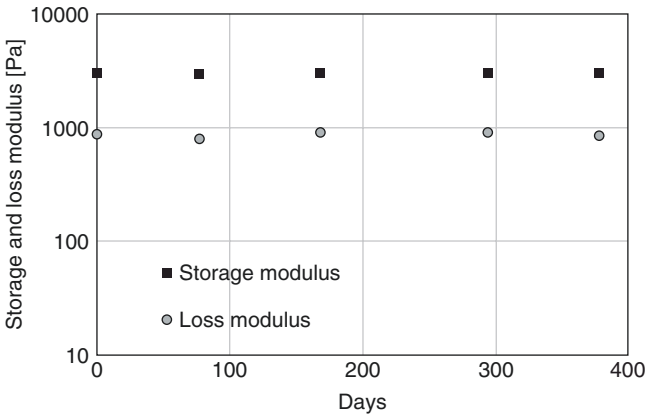

Fig. 39.4 Changes in the mechanical properties of high-viscosity phantom over time

Table 39.6 Results of SWS measurement

	Embedded part		Background part	
	VTIQ	VTQ	VTIQ	VTQ
10 mm	3.0 ± 0.2	2.5 ± 0.0	2.3 ± 0.1	2.0 ± 0.2
20 mm	3.3 ± 0.1	2.8 ± 0.0	2.3 ± 0.1	2.0 ± 0.2
Reference values	3.4 ± 0.2	2.8 ± 0.2	2.3 ± 0.1	2.0 ± 0.2

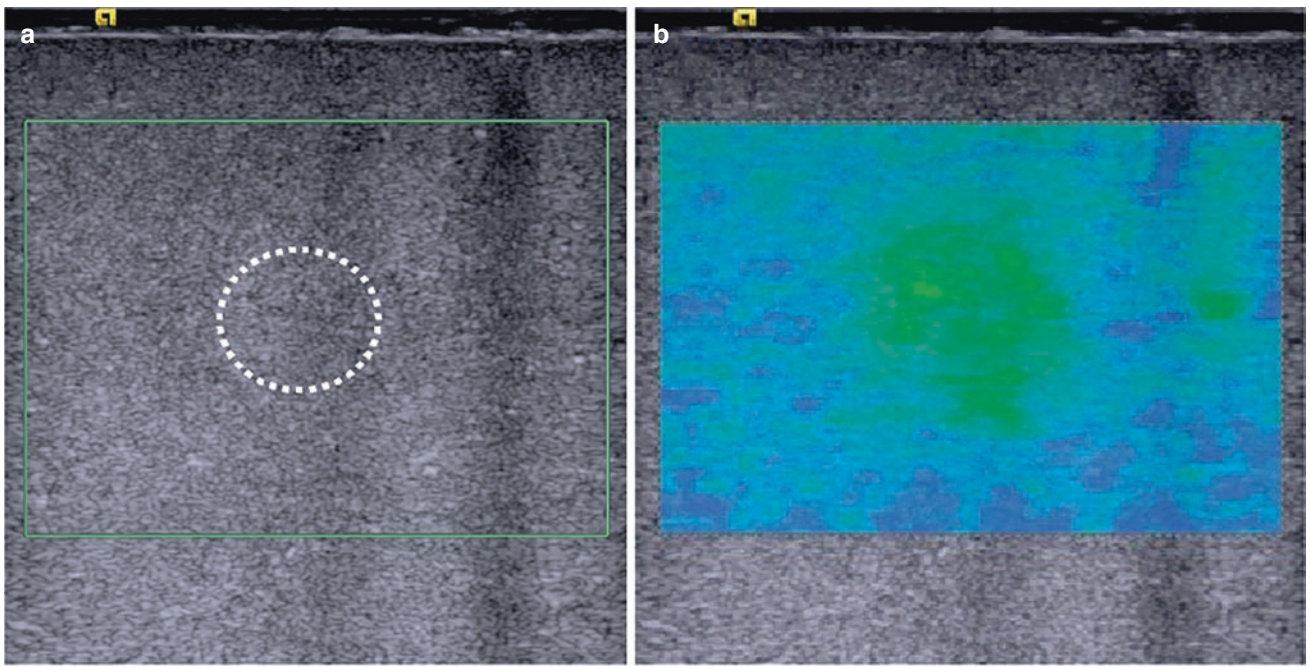

Fig. 39.5 Image of the phantom containing an embedded part with a diameter of 10 mm. (**a**) B mode image. (**b**) VTIQ image

39.3 Conclusion

The purpose of this study was to confirm the frequency characteristics of the developed phantom with commercial USE system and the developed MRE system at multi-scale and multi-frequency. We confirmed that the phantoms are in good agreement with a physical model of the liver, and the developed phantoms are considered effective for the quantitative assessment of the MRE and USE system.

Furthermore, an MRE system using an MR microscope and clinical MRI was developed. We succeeded in performing measurements at multiple frequencies. These developed systems allow quantitative multi-scale and multi-parameter imaging of diseased tissues.

Acknowledgments The viscoelastic evaluation of the phantom was performed under the collaboration of Dr. Takayuki Obata and Dr. Riwa Kishimoto of the National Institute of Radiological Sciences, QST, and Prof. Richard L. Ehman and Prof. Jun Chen of Mayo Clinic in the USA. The ultrasonic characteristics evaluation of the phantom was performed under the collaboration of Prof. Tsuyoshi Shiina and Prof. Makoto Yamakawa of Kyoto University and Prof. Tadashi Yamaguchi of Chiba University. This study was partly supported by JSPS, Grant No. JP17H05279, JP17H02115.

References

1. Muthupillai R, Lomas DJ, Rossman PJ, Greenleaf JF, Manduca A, Ehman RL. Magnetic resonance elastography by direct visualization of propagating acoustic strain waves. Science. 1995;269(5232):1854–7. https://doi.org/10.1126/science.7569924.
2. Parker KJ, Doyley MM, Rubens DJ. Imaging the elastic properties of tissue: the 20 year perspective. Phys Med Biol. 2011;56(1):R1–R29. https://doi.org/10.1088/0031-9155/56/1/R01.
3. Manduca A, Oliphant TE, Dresner MA, Mahowald JL, Kruse SA, Amromin E, Felmlee JP, Greenleaf JF, Ehman RL. Magnetic resonance elastography: non-invasive mapping of tissue elasticity. Med Image Anal. 2001;5(4):237–54. https://doi.org/10.1016/s1361-8415(00)00039-6.
4. Suga M, Matsuda T, Minato K, Oshiro O, Chihara K, Okamoto J, Takizawa O, Komori M, Takahashi T. Measurement of in vivo local shear modulus using MR elastography multiple-phase patchwork offsets. IEEE Trans Biomed Eng. 2003;50(7):908–15. https://doi.org/10.1109/TBME.2003.813540.
5. Suga M, Miura H, Fujiwara T, Tanaka T, Yu Q, Arai K, et al., editors. Inversion algorithm by integral type reconstruction formula for magnetic resonance elastography. Proc Int Soc Magn Reson Med. 2009;2506.
6. Tomita S, Suzuki H, Kajiwara I, Nakamura G, Jiang Y, Suga M, Obata T, Tadano SA. Numerical simulations of magnetic resonance elastography using finite element analysis with a linear heterogeneous viscoelastic model. J Vis. 2017. https://doi.org/10.1007/s12650-017-0436-4
7. Haneishi H, Yamaguchi T, Suga M. Multimodal and multiscale medhical engineering. J Jpn Soc Appl Phys. 2018;87(5):350–6.
8. Quantitative Imaging Biomarkers Alliance. https://www.rsna.org/qiba/
9. Suga M, Mori T, Kishimoto R, Kurokawa T, Abe T, Tsuji H, Obata T. Development of a tissue-simulating viscoelastic gel phantom for MR elastography. Proc Eur Cong Radiol. 2015; https://doi.org/10.1594/ecr2015/C-0757.
10. Ishii K, Suga M, Kishimoto R, Hotta E, Obata T. Development of a tissue-mimicking Visco-elastic phantom for quantitative assessment of MRE. In: First international MRE workshop, vol 49; 2017.
11. Usumura M, Suga M, Kishimoto R, Obata T. Ultrasound-based shear-wave speed measurement on a highly viscous embedded phantom. In: Proceedings of international workshop on advanced imaging technology & international forum on medical imaging in Asia, vol 48; 2019.
12. Kishimoto R, Suga M, Koyama A, Omatsu T, Tachibana Y, Ebner DK, Obata T. Measuring shear-wave speed with point shear-wave elastography and MR elastography: a phantom study. BMJ Open. 2017;7(1):e013925. https://doi.org/10.1136/bmjopen-2016-013925en.
13. Asbach P, Klatt D, Schlosser B, Biermer M, Muche M, Rieger A, Loddenkemper C, Somasundaram R, Berg T, Hamm B, Braun J, Sack I. Viscoelasticity-based staging of hepatic fibrosis staging of hepatic fibrosis elastography. Radiology. 2010;257(1):80–6. https://doi.org/10.1148/radiol.10092489.